Journal of Alloys and Compounds 509 (2011) 3638–3643

Contents lists available at ScienceDirect

Journal of Alloys and Compounds

journal homepage: www.elsevier.com/locate/jallcom

# Preparation of $BaMgAl_{10}O_{17}:Eu^{2+}$ phosphor with small particle size by co-precipitation method

Yan Dong*, Zhisen Wu, Xuelin Han, Rong Chen, Weijie Gu

*School of Material Science and Engineering, SouthEast University, 2 Sipailou, Nanjing 210096, China*

ARTICLE INFO

*Article history:*
Received 21 June 2010
Received in revised form
16 December 2010
Accepted 17 December 2010
Available online 23 December 2010

*Keywords:*
Precipitation
Phosphors
X-ray diffraction

ABSTRACT

A $BaMgAl_{10}O_{17}:Eu^{2+}$ phosphor with fine particle size was synthesized by a chemical co-precipitation method. Co-precipitation of $Ba^{2+}$, $Al^{3+}$, $Mg^{2+}$, and $Eu^{2+}$ was achieved under precisely controlled precipitation conditions. The $Al^{3+}$ ions were precipitated as ammonium aluminum carbonate hydroxide (AACH). Phase transition and particle growth processes of the precipitate mixture during calcining process were investigated, and the formation mechanism of the $BaMgAl_{10}O_{17}$ phase was discussed. The results show that the formation temperature of the $BaMgAl_{10}O_{17}$ phase in the co-precipitation mixture was significantly lower than that of a high temperature solid state reaction method. The $BaMgAl_{10}O_{17}$ phase was formed from the reaction between the $BaAl_2O_4$ phase and $\gamma$-$Al_2O_3$ phase; no $\alpha$-$Al_2O_3$ phase appeared during the entire process. Well-dispersed $BaMgAl_{10}O_{17}:Eu^{2+}$ phosphor powder in the form of hexagonal flakes with small particle size (1–2 μm) could be prepared by this method.



## 1. Introduction

$Eu^{2+}$ activated barium magnesium aluminate blue phosphor ($BaMgAl_{10}O_{17}:Eu^{2+}$, BAM) is used for plasma display panel (PDP) and fluorescent lamps due to its high efficiency and excellent color coordinates. The BAM phosphor has been an important focus in the field of luminescent materials [1–7].

The particle size and morphology of phosphors have become more important properties besides luminescence efficiency thanks to the increasing demand of high resolution displays. In the case of PDP, the reduction of particle size of phosphor can increase the area of actual light-emission, which improves efficiency. Commercial BAM blue phosphor for PDP is usually prepared by the high-temperature solid state reaction method, i.e., mixing $\alpha$-$Al_2O_3$, MgO, $BaCO_3$, $Eu_2O_3$ and fluxes together, and calcining in a reducing atmosphere at 1500–1600 °C. Phosphors made by this method have to be sintered, and coarse particles need to be treated by milling, which damages luminescence performance. So far, BAM blue phosphor with both excellent luminescence properties and particle size less than 3 μm is not commercially available.

The performance of phosphors is not improved beyond a certain size reduction. Phosphor particles such as nanophosphors have poor luminescence performance because of the non-negligible proportion of an inactive surface layer. Similarly, phosphor particles which have many defects such as grain boundaries are not a good option, either. Optimal phosphor particles should have a particle size of 1–2 μm [8,9], be well-crystallized (preferably single crystal particles), and have a good dispersion in the slurry.

New synthesis methods have been developed in recent years to reduce the particle size of the aluminate phosphors and also to improve the particle morphology [10–25]. Sol–gel technique was introduced to obtain fine phosphor particles; Wang et al. prepared BAM nanorods by this method [11]. In addition, Wang et al. applied a nanocoating process to synthesize homogeneous BAM phosphor with high luminescence intensity [13]. Chen et al. prepared pure and well-crystallized BAM nanoscale blue phosphors by the microwave-induced solution combustion synthesis method [14]. Compared with these methods, the chemical co-precipitation method is more promising in achieving small and well-crystallized phosphor particles [26,27], and is already commercialized in the preparation of $Y_2O_3:Eu^{3+}$ phosphor.

However, there are great difficulties when synthesizing aluminate phosphors by the chemical precipitation method. One challenge is the problem of the precipitation state of $Al^{3+}$. These ions readily precipitate in the form of $\gamma$-AlO(OH) boehmite, which turn to a hard agglomerated mass after calcining or even only after drying. The final particles sinter together with an irregular shape. Particle agglomeration is much more severe than that achieved by a high-temperature solid state method. Except for the obstacle of the precipitation state of $Al^{3+}$, the precipitates are likely to be transformed into nanoparticle aggregates. A phosphor prepared from the nano particles has poor luminescence performance

* Corresponding author. Tel.: +86 25 52090634; fax: +86 25 52090634.
*E-mail address:* dongyan@seu.edu.cn (Y. Dong).

0925-8388/$ – see front matter © 2010 Elsevier B.V. All rights reserved.
doi:10.1016/j.jallcom.2010.12.127

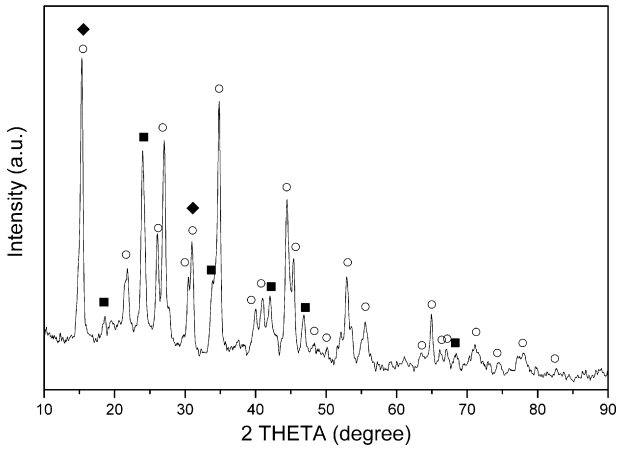


**Fig. 1.** XRD pattern of the precipitates.

because of the presence of surface layers and boundaries in large quantities.

In this study, the precipitates and the high-temperature calcining process of a chemical co-precipitation method for $BaMgAl_{10}O_{17}$ phase are investigated, and the preparation of the BAM phosphor with small particle size as well as high luminescence efficiency is reported.

## 2. Materials and methods

The reagents $Al(NO_3)_3{\cdot}9H_2O$ (spectral purity), $Mg(NO_3)_2$ (analytical grade), $Ba(NO_3)_2$ (analytical grade), and $Eu_2O_3$ (99.999%) powders were weighed according to the stoichiometry of $Ba_{0.95}Eu_{0.05}MgAl_{10}O_{17}$, and were dissolved in de-ionized water to prepare a solution containing metal ions. A solution of 2–3 mol/L $NH_4HCO_3$ (analytically pure) was prepared with de-ionized water, and $NH_4F$ was added to the solution [0.2–0.4 g $NH_4F$ per 100 g $Al(NO_3)_3{\cdot}9H_2O$]. The $NH_4HCO_3$ solution was heated at 20–50 °C while controlling the pH value at 8–10. The metal ion solution was added into the $NH_4HCO_3$ solution in drops while stirring. The precipitate was centrifuged, and the supernatant was discarded. A light loose white powder could be obtained after drying the precipitate.

The $BaMgAl_{10}O_{17}:Eu^{2+}$ phosphor was prepared by calcining the white precipitate powder at 1200 °C for 1 h, reducing the fired powder at 1400–1500 °C in a weakly reducing $N_2$–$H_2$ atmosphere for 2–3 h, and then dispersing the powder by weak milling. Weak milling slightly changed the luminescence efficiency.

The structures of the precipitates and the calcined powder samples were characterized by X-ray diffraction (Shimadzu, XD-3A) with Cu Kα. The particle morphology of the precipitate and the phosphor were inspected using a field emission scanning electron microscope (FEI, Sirion-400). The energy dispersive X-ray spectra (EDS) were also obtained using this instrument. The emission spectra were obtained on a PDP-VUV fluorescence spectroradiometric system (SENSING Instruments). The particle size distribution was measured by a laser particle size analyzer (Jinan Winner, 2000A).

## 3. Results and discussion

### 3.1. Precipitation forms of $Al^{3+}$, $Ba^{2+}$, and $Mg^{2+}$

During the co-precipitation of $Al^{3+}$, $Ba^{2+}$, $Mg^{2+}$ and $Eu^{3+}$ ions, feed concentration, precipitant concentration, temperature, and pH value were important factors. The parameters of the co-precipitation reaction were similar to those of the preparation of small particle size $A_2O_3$ powder, only stricter. A more detailed information can be seen in previous reports [28,29].

The X-ray diffraction pattern of the precipitates is shown in Fig. 1, in which "○" represents the AACH phase (JCPDS 76-1923),"■" represents the $BaCO_3$ phase (JCPDS 71-2394), and "♦" represents the $Mg_5(CO_3)_4(OH)_2{\cdot}4H_2O$ (JCPDS 25-0513) phase. As indicated in Fig. 1, $Al^{3+}$ ions were precipitated as AACH, and the $Ba^{2+}$ ions existed as $BaCO_3$. Diffraction peaks of the precipitation phase of $Eu^{2+}$ were difficult to identify because of its low content.

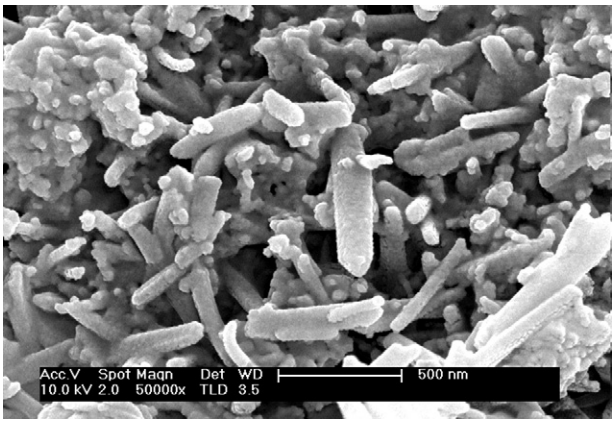


**Fig. 2.** SEM photograph of the precipitates.

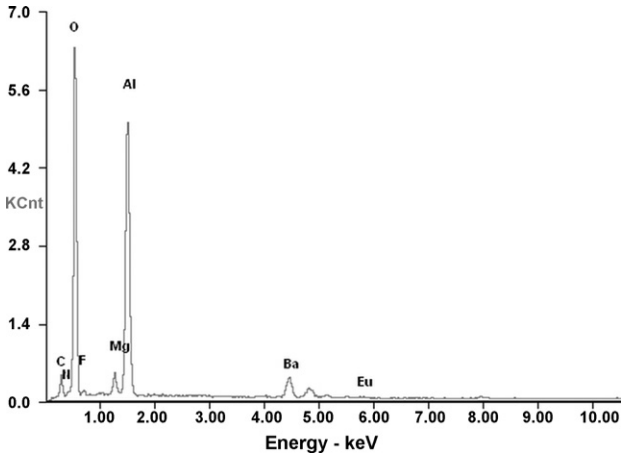


**Fig. 3.** EDS spectrum of the precipitates.

Diffraction peaks of the precipitation phase of $Mg^{2+}$ ions were also difficult to identify. The content of Mg was small, and the two main diffraction peaks of $Mg_5(CO_3)_4(OH)_2{\cdot}4H_2O$ overlapped with two diffraction peaks ($2\theta = 15°$, 31°) of AACH. The precipitation phase of $Mg^{2+}$ was verified by experiments on precipitating $Mg^{2+}$ alone with the same parameters.

Fig. 2 is the SEM photograph of the precipitates. The co-precipitation product mostly consisted of rod-like particles, and had spherical particles among the rod-like particles. The diameter of the rod was approximately 60–80 nm. The rod-like particles were AACH [28].

Fig. 3 and Table 1 are the EDS results of the precipitates. Elemental Mg was found in the EDS spectrum; however, the existence of Eu could not be proven since its content was extremely low.

### 3.2. Phase transformation during the calcining process

The dried precipitates were calcined at 400, 600, 700, 800, 900, 1000, 1100, 1200, and 1300 °C for 1 h, and the products were analyzed by XRD, as shown in Fig. 4. Here, "○" represents the

**Table 1**
Composition of the precipitates determined by EDS analysis.

| | Element | | | | | | | |
|---|---|---|---|---|---|---|---|---|
| | C | N | O | F | Mg | Al | Ba | Eu |
| Wt% | 13.04 | 03.18 | 49.84 | 01.47 | 01.76 | 22.67 | 07.58 | 00.47 |
| At% | 19.83 | 04.14 | 56.89 | 01.41 | 01.33 | 15.34 | 01.01 | 00.06 |

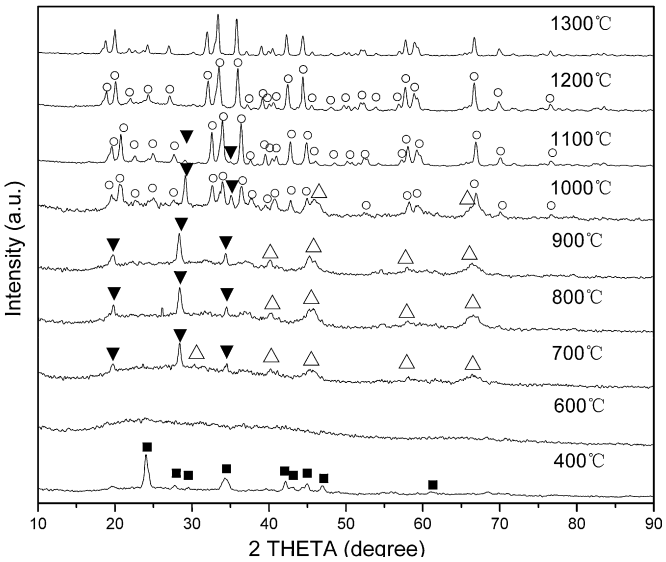


**Fig. 4.** XRD patterns of samples of calcining the precipitates at different temperatures.

$BaMgAl_{10}O_{17}$ phase (JCPDS 26-0163), "■" represents the $BaCO_3$ phase (JCPDS 71-2394), "△" represents the γ-$Al_2O_3$ phase (JCPDS 10-0425), and "▼"' represents the $BaAl_2O_4$ phase (JCPDS 17-0306).

The AACH phase decomposed when calcining the precipitates at 400 °C. The reaction that took place is $2NH_4AlO(OH)HCO_3 \rightarrow Al_2O_3 + 2CO_2\uparrow + H_2O\uparrow + NH_3\uparrow$. The volume of the sample was significantly reduced due to the loss of $NH_3$, $H_2O$ and $CO_2$. Alumina existed as an amorphous state at this temperature. Only diffraction peaks of the $BaCO_3$ phase were found. No phases with Mg appeared in the XRD pattern.

An unexpected phenomenon occurred when calcining the precipitates at 600 °C because no obvious diffraction peaks were found. The precipitation phase of $Al^{3+}$ was amorphous alumina just as it existed at 400 °C. The $BaCO_3$ phase disappeared, however, and no other phases of $Ba^{2+}$ or $Mg^{2+}$ were found. Mg might exist within the amorphous alumina. Chen and Yan reported a similar state when they calcined BAM samples at 800 °C using a sol–gel route [17]. The diffusion mechanism and the status of Ba and Mg were currently unclear.

$BaAl_2O_4$ phase and γ-$Al_2O_3$ phase were found in the sample calcined at 700 °C. This indicated that Ba and $Al_2O_3$ began to react at this temperature. The amorphous alumina also started to transform to the γ-$Al_2O_3$ phase, which is a crystal with poor crystallinity and many defects [30,31]. The diffraction peaks attributed to the

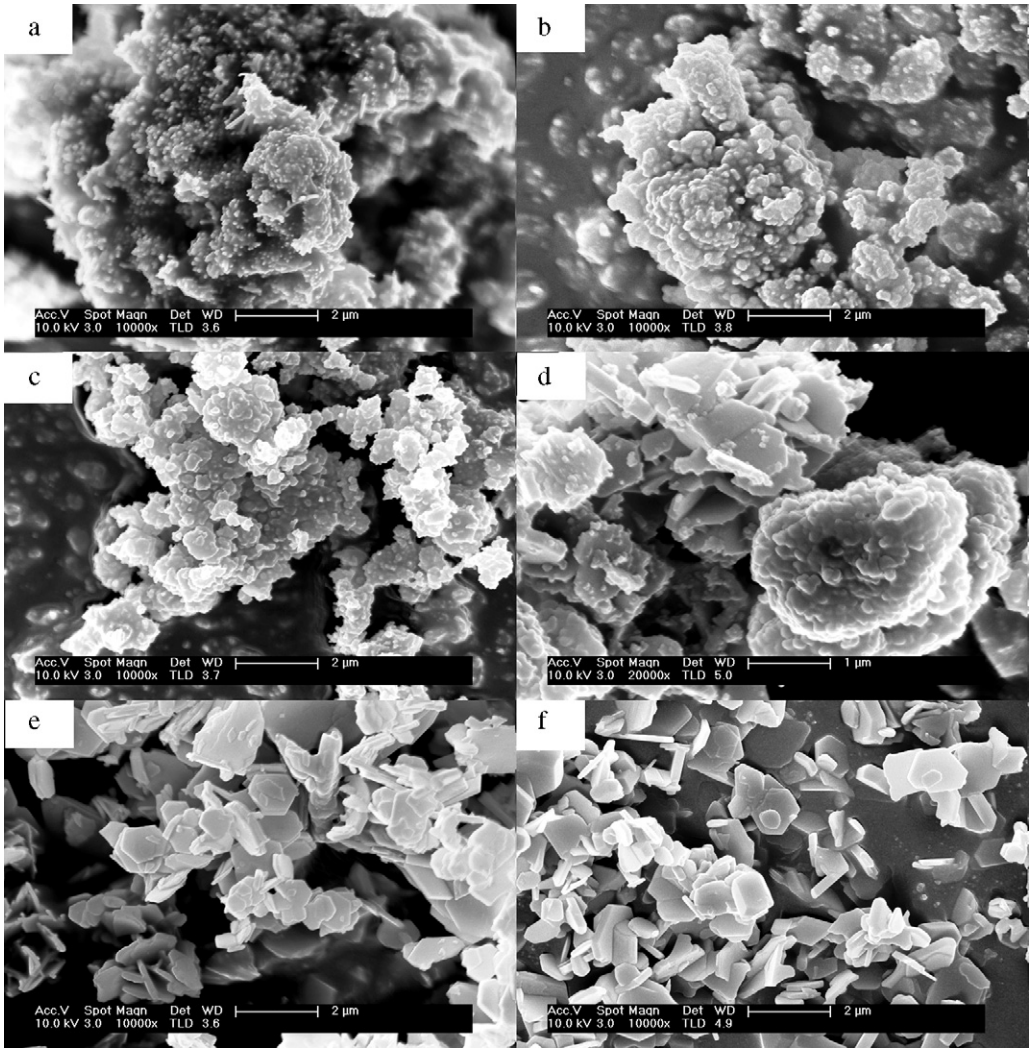


**Fig. 5.** SEM photographs of samples of calcining the precipitates at (a) 600 °C, (b) 900 °C, (c) 1000 °C 10000×, (d) 1000 °C 20000×, (e) 1100 °C, and (f) 1200 °C.

$BaAl_2O_4$ phase became stronger as the temperature increased, but new phases were detected in the samples till 900 °C.

$BaMgAl_{10}O_{17}$ phase (JCPDS 26-0163) was formed when the precipitates were calcined at 1000 °C. The $BaAl_2O_4$ phase and γ-$Al_2O_3$ phase coexisted with the $BaMgAl_{10}O_{17}$ phase at this temperature.

The intensity of the diffraction peaks of $BaMgAl_{10}O_{17}$ phase increased after calcining at 1100 °C, and while the intensity of $BaAl_2O_4$ phase and γ-$Al_2O_3$ phase decreased. The $BaMgAl_{10}O_{17}$ particles gradually formed, and the amount of $BaAl_2O_4$ and γ-$Al_2O_3$ decreased because of the reaction. Some $BaAl_2O_4$ phase and γ-$Al_2O_3$ phase remained at this temperature, which meant that the reaction was not completed yet.

The diffraction peaks of the $BaAl_2O_4$ phase and γ-$Al_2O_3$ phase disappeared in the sample calcined at 1200 °C. Pure $BaMgAl_{10}O_{17}$ phase was formed at this temperature. No changes could be observed when the temperature was increased to 1300 °C or higher.

Compared with the phase transformation process of the conventional high temperature solid state reaction method [29], the process of co-precipitation method showed large differences:

(1) The synthesis temperature of the $BaMgAl_{10}O_{17}$ phase was lowered by about 200 °C, which was related to the uniform composition and the addition of $F^-$ ions. Lower synthesis temperature greatly reduced the particle agglomeration during the high-temperature process. It was beneficial for preparing a BAM phosphor of small particle size.
(2) The $BaMgAl_{10}O_{17}$ phase was formed directly from the reaction between the $BaAl_2O_4$ phase and γ-$Al_2O_3$ phase (with Mg), and no α-$Al_2O_3$ phase appeared during the entire synthesis process. While in the high-temperature solid state reaction process, Ba, Mg, and Eu diffused into α-$Al_2O_3$ particles with the assistance of a flux. Therefore, the size, morphology, and reaction activity of α-$Al_2O_3$ particles were essential on the final performance of the BAM phosphor [29]. However, there was no α-$Al_2O_3$ phase in the co-precipitation process.

### 3.3. Variation of the particle morphology during calcining process

The SEM photographs of samples after 600, 700, 900, 1100, and 1200 °C calcining are shown in Fig. 5. Rod-like particles no longer existed when the precipitates were calcined at 600 °C, but were replaced by an amorphous state. Combining with the XRD analysis from the previous section, the sample appears to be amorphous alumina with Ba and Mg.

The particle morphology changed in the sample calcined at 900 °C. Many small, round particles were present on the surface of the big particles. However, the big particles still did not have any crystalline morphology. The $BaAl_2O_4$ phase and γ-$Al_2O_3$ phase were formed at 900 °C, according to the XRD from the previous section.

Most particles retained their shape after calcining at 1000 °C. However, a small amount of flaky particles appeared at this temperature, as shown in Fig. 5(d). These flaky particles are the grains of the $BaMgAl_{10}O_{17}$ phase, according to the XRD pattern. This indicates that the nucleation of $BaMgAl_{10}O_{17}$ phase already began at 1000 °C.

A large number of flaky particles with regular hexagonal shape appeared at 1100 °C. The XRD analysis confirms that the main phase was $BaMgAl_{10}O_{17}$ at this temperature. A small quantity of $BaAl_2O_4$ phase also remained. Therefore, the hexagonal flaky particles are $BaMgAl_{10}O_{17}$. When the calcining temperature was increased to 1200 °C, the shape and the size of $BaMgAl_{10}O_{17}$ particles were slightly changed.

The $BaMgAl_{10}O_{17}$ particles prepared by this method were apparently smaller than those produced by the high temperature solid state method. No serious agglomeration occurred in the powder. The mean size of $BaMgAl_{10}O_{17}$ particles could be easily dispersed to 1–2 μm, which is a significant improvement compared with the traditional method.

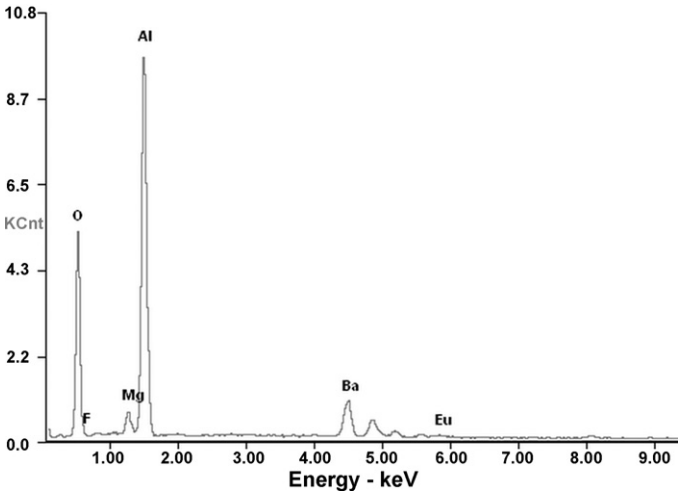


**Fig. 6.** EDS spectrum of the sample of calcining the precipitates at 1200 °C.

Fig. 6 shows the EDS spectrum of the sample calcined at 1200 °C, in which Al, Mg, Ba, Eu, and F were examined. The existence of elemental Eu could also be verified by the luminescence of the reduced sample, because Eu is the source of luminescence in BAM phosphor. Table 2 reveals the element ratio of the sample estimated by EDS, in which the ratio of Al, Mg, and Ba corresponded to the stoichiometric proportion of $BaMgAl_{10}O_{17}$.

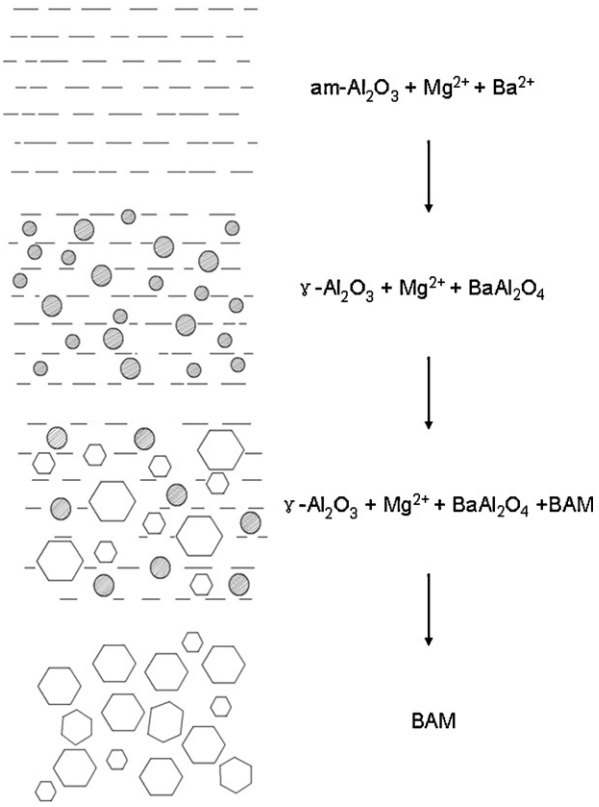


**Fig. 7.** Schematic diagram of the formation of the $BaMgAl_{10}O_{17}$ phase.

**Table 2**
Composition of the 1200 °C calcined sample determined by EDS analysis.

| | Element | | | | | |
|---|---|---|---|---|---|---|
| | O | F | Mg | Al | Ba | Eu |
| Wt% | 32.60 | 00.14 | 03.55 | 40.69 | 21.60 | 01.41 |
| At% | 52.70 | 00.19 | 03.78 | 39.01 | 04.07 | 00.24 |

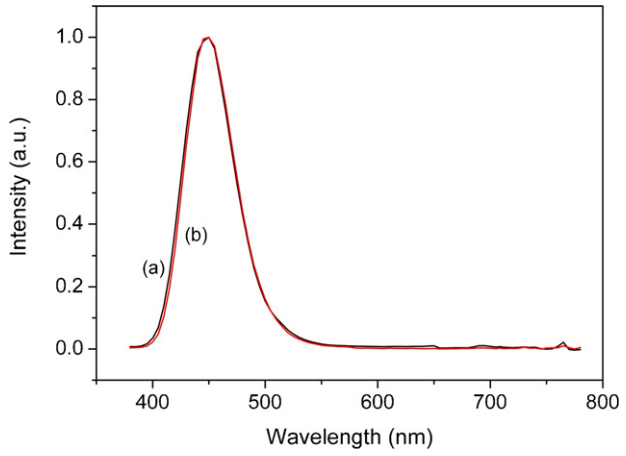


**Fig. 8.** Emission spectra of BAM phosphor prepared by (a) co-precipitation method and (b) high-temperature solid state method.

### 3.4. Formation mechanism of the $BaMgAl_{10}O_{17}$ phase

As shown in Sections 3.2 and 3.3, the formation process of BAM phosphor prepared by the co-precipitation process was very different from that of the conventional high-temperature solid state method. Considering the phase transformation process and the variation of the particle morphology, a possible formation mechanism of the $BaMgAl_{10}O_{17}$ phase was given, as shown in Fig. 7.

The precipitates first decomposed and turned into a uniform state after calcining. This is a state of amorphous alumina with $Mg^{2+}$ and $Ba^{2+}$ distributed in it.

The amorphous $Al_2O_3$ converted to the γ-$Al_2O_3$ phase as the calcining temperature was increased. The γ-$Al_2O_3$ phase is a crystal with many defects [20,21]. The $Mg^{2+}$ might exist in γ-$Al_2O_3$ in one form or another, for example, trapped in the defects. The $Ba^{2+}$ and γ-$Al_2O_3$ started to react, and the $BaAl_2O_4$ phase was formed. The size of the $BaAl_2O_4$ particles was small, measuring up to only dozens of nanometers. As a result, the distances between $Al^{3+}$ ions, $Mg^{2+}$ ions and $BaAl_2O_4$ particles were short, which ensured high reactivity.

When the calcination temperature reached around 1000 °C, $BaAl_2O_4$ particles reacted with the surrounding $Al^{3+}$ ions and $Mg^{2+}$ ions, i.e., the nucleation of the $BaMgAl_{10}O_{17}$ crystal started. The $BaMgAl_{10}O_{17}$ particles grew gradually, and the amount of $BaAl_2O_4$ and γ-$Al_2O_3$ decreased due to the reaction. The reaction ceased when the temperature was increased to 1200 °C.

During the above-mentioned $BaMgAl_{10}O_{17}$ formation process, the mass transfer distance was very short and the nucleation rate was very high. The temperature range of the nucleation and growth $BaMgAl_{10}O_{17}$ crystals by the co-precipitation method was narrow. Numerous grains nucleated and grew simultaneously. The growth of $BaMgAl_{10}O_{17}$ grains ended when one of the reactants was exhausted, such as $BaAl_2O_4$ or γ-$Al_2O_3$. The grain size slightly changed when the calcining temperature was increased.

The situation is quite different in a high temperature solid state reaction process. In this case, the Ba in $BaCO_3$ particles and Mg in MgO particles diffuse into surrounding α-$Al_2O_3$ particles [22,23]. Long-distance diffusion needs extremely high temperature and long reaction time. In most cases, it needs the assistance of a flux, which will introduce a liquid phase and will result in serious agglomeration. For this reason, BAM phosphor prepared by the high-temperature solid state method usually has coarse particles.

Moreover, the two methods are different in the formation mechanism of the $BaMgAl_{10}O_{17}$ crystal.

The $BaMgAl_{10}O_{17}$ phase is a typical β-$Al_2O_3$ structure. The unit cell of $BaMgAl_{10}O_{17}$ consists of two spinel blocks ($MgAl_{10}O_{16}$) and one mirror plane (BaO) [32].

In the case of the high temperature solid state method, the reaction phases are α-$Al_2O_3$, MgO, and $BaCO_3$. The stable corundum crystal needs a structural change, and Mg and Ba elements need to diffuse through a long distance. Therefore, a strong driving force is required, which usually means a high temperature and the assistance of a flux.

However, during the process of the co-precipitation method, the reaction phases were γ-$Al_2O_3$ (with Mg) and $BaAl_2O_4$. The γ-

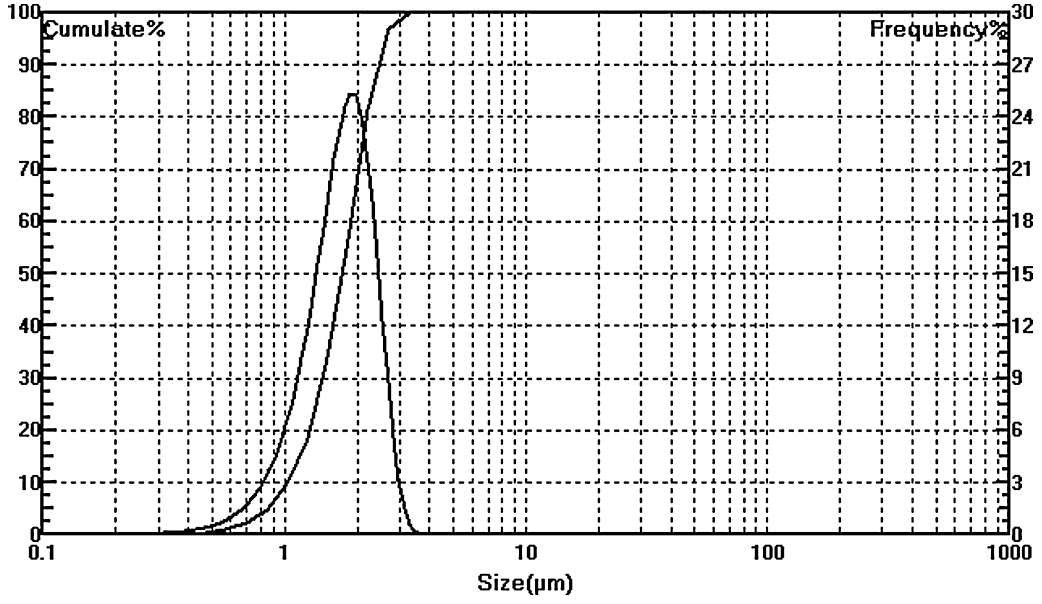


**Fig. 9.** Particle size distribution of the BAM phosphor.

$Al_2O_3$ phase is a defective spinel structure [20,21], which is similar to the structure of the spinel blocks in $BaMgAl_{10}O_{17}$. The crystal reconstruction from γ-$Al_2O_3$ to the $MgAl_{10}O_{16}$ spinel block is easier than that from α-$Al_2O_3$. Therefore, $BaMgAl_{10}O_{17}$ crystals could nucleate at a temperature of about 1000 °C. The γ-$Al_2O_3$ phase did not even change into the α-phase at this temperature. Correspondingly, the nucleation of $BaMgAl_{10}O_{17}$ crystal became easier.

Low reaction temperature, high nucleation rate, and short diffusion distance are the main reasons for attaining small $BaMgAl_{10}O_{17}$ particles by a co-precipitation method.

Continuous research on the mechanism of $BaMgAl_{10}O_{17}$ phase formation, the role of $F^-$ ions, and the crystal growth mechanism are now underway.

### *3.5. Luminescence performance and particle size distribution of the BAM phosphor prepared by the co-precipitation method*

The emission spectrum of the BAM phosphor was measured by excitation under vacuum ultraviolet light. As a comparison, a BAM phosphor prepared by the high-temperature solid state method was also measured. The results are shown in Fig. 8. The BAM phosphor made by the co-precipitation method showed high luminescence. The luminescence intensity and the spectral properties of the sample were almost the same with the one produced by the high-temperature solid state method.

Fig. 9 shows the particle size distribution of the BAM phosphor prepared by the co-precipitation method. The center particle size $D_{50}$ of the sample was 1.74 μm, with a narrow distribution range. The particle size of 1–2 μm is sufficient to meet the demand for future high-definition PDP.

## 4. Conclusions

A $BaMgAl_{10}O_{17}:Eu^{2+}$ phosphor with fine particle size and high luminescence performance was synthesized by a chemical co-precipitation method. Unlike the process of a high-temperature solid state method, $BaMgAl_{10}O_{17}$ nucleated directly from the reaction between $BaAl_2O_4$ and γ-$Al_2O_3$ (with Mg), and no α-$Al_2O_3$ phase appeared during the entire synthesis. The synthesis temperature was distinctly lowered. Small dispersed particles were achieved because of the short diffusion distance and the high nucleation rate. The method is promising for preparing high-efficiency and small-size aluminate phosphors for high definition PDP.

## Acknowledgements

This work was supported by the Natural Science Foundation of Jiangsu Province (BK2008317) and the Cultivation Fund of the Key Scientific and Technical Innovation Project, Ministry of Education of the People's Republic of China (No. 707029). We are also deeply grateful to Prof.Adrian Kitai at McMaster University for his kind help in the revision of this manuscript.

## References

[1] Z. Chen, Y.W. Yan, J.-M. Liu, Y. Yin, H. Wen, G. Liao, C. Wu, J. Zao, D. Liu, H. Tian, C. Zhang, S. Li, J. Alloys Compd. 478 (2009) 679–683.
[2] E. Zycha, W. Goetz, N. Harrit, H. Spanggaard, J. Alloys Compd. 380 (2004) 113–117.
[3] B. Moine, G. Bizarri, Opt. Mater. 28 (2006) 587–591.
[4] R. Turos-Matysiak, M. Grinberg, J.W. Wang, W.M. Yen, R.S. Meltzer, J. Lumin. 122–123 (2007) 107–109.
[5] Y.K. Jeong, H.-J. Kim, H.G. Kim, B.-H. Choi, Curr. Appl. Phys. 9 (2009) S249–S251.
[6] Z.H. Zhang, Y.H. Wang, X.X. Lia, Y.K. Du, W.J. Liu, J. Lumin. 122–123 (2007) 1003–1005.
[7] Z.H. Zhang, Y.H. Wang, X.X. Li, J. Alloys Compd. 478 (2009) 801–804.
[8] J.P. Boeuf, J. Phys. D: Appl. Phys. 36 (2003) R53–R79.
[9] H. Bechtel, T. Justel, H. Glaser, D.U. Wiechert, J. SID 10 (2002) 63–67.
[10] P. Zhu, W. Di, Q. Zhu, B. Chen, H. Zhu, H. Zhao, Y. Yang, X. Wang, J. Alloys Compd. 454 (2008) 245–249.
[11] Z. Wang, Y. Wang, Y. Li, B. Liu, J. Alloys Compd. 509 (2011) 343–346.
[12] B.M. Mothudi, O.M. Ntwaeaborwa, S.S. Pitale, H.C. Swart, J. Alloys Compd. 508 (2010) 262–265.
[13] J. Wang, G. Ning, W. Pan, X. Yang, Y. Lin, Mater. Sci. Eng. B 147 (2008) 43–46.
[14] Z. Chen, Y. Yan, J. Liu, Y. Yin, H. Wen, J. Zao, D. Liu, H. Tian, C. Zhang, S. Li, J. Alloys Compd. 473 (2009) L13–L16.
[15] K.-T. Kuo, S.-P. Lee, S.-Y. Chen, J. Phys. Chem. Solids 69 (2008) 362–365.
[16] J.G. Mahakhode, S.J. Dhoble, C.P. Joshi, S.V. Moharil, J. Alloys Compd. 438 (2007) 293–297.
[17] Z. Chen, Y. Yan, Mater. Lett. 61 (2007) 3927–3930.
[18] S.H. Lee, H.Y. Koo, D.S. Jung, J.H. Yi, Y.C. Kang, Ceram. Int. 35 (2009) 2651–2657.
[19] C.W. Won, H.H. Nersisyan, H.I. Won, S.J. Kwon, H.Y. Kim, S.Y. Seo, J. Lumin. 130 (2010) 678–681.
[20] D.-K. Kim, S.-H. Hwang, I.-G. Kim, J.-C. Park, S.-H. Byeon, J. Solid State Chem. 178 (2005) 1414–1421.
[21] L.-T. Chen, I.-L. Sun, C.-S. Hwang, S.-J. Chang, J. Lumin. 118 (2006) 293–300.
[22] H. Chang, W. Lenggoro, T. Ogi, K. Okuyama, Mater. Lett. 59 (2005) 1183–1187.
[23] J. Zhou, Y. Wang, B. Liu, Y. Lu, J. Alloys Compd. 484 (2009) 439–443.
[24] Z. Chen, Y. Yan, Physica B 392 (2007) 1–6.
[25] C.-H. Lu, C.-H. Huang, B.-M. Cheng, J. Alloys Compd. 473 (2009) 376–381.
[26] J. Su, Q.L. Zhang, S.F. Shao, W.P. Liu, S.M. Wan, S.T. Yin, J. Alloys Compd. 470 (2009) 306–310.
[27] Z.H. Zhang, Y.H. Wang, Mater. Lett. 61 (2007) 4128–4130.
[28] Z. Wu, Y. Shen, Y. Dong, J. Jiang, J. Alloys Compd. 467 (2009) 600–604.
[29] Z. Wu, Y. Dong, J. Jiang, J. Alloys Compd. 467 (2009) 605–610.
[30] G. Gutieĭrrez, A. Taga, B. Johansson, Phys. Rev. B 65 (2001) 012101.
[31] G. Paglia, C.E. Buckley, A.L. Rohl, Phys. Rev. B 68 (2003) 144110.
[32] V. Pike, S. Samuel Patraw, A.L. Diaz, B.G. DeBoer, J. Solid State Chem. 173 (2003) 359–366.